

Curriculum Vitae

Name: Venkatakrisnan Veerasubramanian

Permanent Address: D-137, Balaji Street, Alagappan Nagar, Madurai
625003, India

Degree and date to be conferred: Master of Science, May 2008

Date of Birth: May 31, 1984

Place of Birth: Trivandrum, India

Education:

M.S Electrical Engineering, Major: Photonics
University of Maryland Baltimore County, 2008.

B.E Electrical and Electronics Engineering
Birla Institute of Technology and Science, Pilani, India, 2005.

Professional publications:

1. V. Veerasubramanian, J. Hu, J. Zweck, and C. R. Menyuk, "Propagation analysis of an 80-Gb/s wavelength-converted signal utilizing XPM," in Proc. Conference on Optical Fiber Communications (OFC), San Diego, CA, paper JWA69, (2008).

Professional positions held:

Teaching Assistant, Dept. of CSEE, UMBC, (August 2005 – December 2007).

Intern, Texas Instruments, Bangalore, India (January 2005 – July 2005).

Abstract

Title of Thesis: Propagation analysis of an 80-Gb/s wavelength-converted signal utilizing cross-phase modulation

Venkatakrisnan Veerasubramanian, Master of Science, 2008

Thesis directed by: Professor Curtis R. Menyuk

Computer Science and Electrical Engineering

For robust operation of high speed networks, wavelength conversion, as well as new signal processing and coding techniques are important. In this thesis, we model the propagation of an 80-Gb/s wavelength-converted signal generated by utilizing cross-phase modulation (XPM) in a highly nonlinear fiber. We then compare the transmission performance of the wavelength-converted signal to that of the standard signal. After propagation over 1280 km or less, wavelength conversion adds no signal degradation in terms of BER. We conclude that wavelength conversion leads to no significant deterioration in a noise-limited propagation system.

**Propagation analysis of an
80-Gb/s wavelength-converted signal
utilizing cross-phase modulation**

by

Venkatakrishnan Veerasubramanian

Thesis submitted to the Faculty of the Graduate School
of the University of Maryland in partial fulfillment
of the requirements for the degree of
Master of Science

2008

© Copyright by Venkatakrisnan Veerasubramanian, 2008

Acknowledgements

I would like to thank my research advisor and *Guru*, Professor Curtis R. Menyuk, for his excellent guidance and constant support through the course of my graduate life at UMBC. I learnt a lot of essential skills through his constructive criticisms, both academic, as well as social. No wonder Indian culture places ones' teacher at a much higher pedestal compared to even God.

It was a great pleasure to work with great scientists and enthusiastic individuals, Professor John Zweck, Professor Gary Carter and Dr. Vladimir Grigoryan. Several discussions with John and Vladimir played a major part in progressing forward with this study.

Being a part of a closely-knit research group has helped me learn and think from various viewpoints. I am thankful to my labmate for more than two years, Jonathan Hu, with whom there were many scintillating moments. I am also grateful to Dr. Oleg Sinkin, Vlad Seghete and Anisuzzaman Talukder.

I express my gratitude to my parents and family members for being by my side always. This thesis is dedicated to my parents. I am also indebted to my friends Palani, Achuth, Srihari, and Sandeep, as well as the entire Bazookz gang, who have made my stay in the US a cherishable one.

TABLE OF CONTENTS

1. Introduction	1
2. Fiber nonlinearities	4
2.1 Self-phase modulation	8
2.2 Cross-phase modulation	9
2.3 Four-wave mixing	11
2.4 Propagation of light in optical fibers	13
3. Wavelength conversion	15
3.1 Optoelectronic regeneration	16
3.2 Optical gating techniques	17
3.3 Wave-mixing techniques	19
3.4 Fiber-based wavelength conversion	21
4. Wavelength conversion using cross-phase modulation	24
4.1 Small-signal model	25
4.2 Calculation of the bit-error ratio	29
4.3 The semi-analytical receiver model	31
4.4 Simulation setup	33
4.5 Setting up the computational window	37

4.6 Results and analysis	37
5. Conclusions	42
Appendix A: List of acronyms	44
Bibliography	46

LIST OF FIGURES

3.1	Schematic of the three typrs of opto-electronic regeneration: (a) 1R: re-amplification, (b) 2R : re-amplification and reshaping, and (c) 3R: re-amplification, reshaping, and retiming. Reproduced from [2].	17
3.2	Schematic of the wavelength conversion technique utilizing cross-gain modulation in semiconductor optical amplifiers.	18
3.3	Schematic of a wavelength converter utilizing four-wave mixing in a semiconductor optical amplifier.	20
3.4	Experimental setup of the all-optical wavelength converter showing the MUX-DEMUX links. Reproduced from [24].	22
4.1	Simulation setup for the small-signal model	25
4.2	Conversion efficiency as a function of fiber distance for varying pump powers (a) 10 dBm, (b) 6 dBm, and (c) 0 dBm. The circles indicates results obtained using the split-step Fourier method, while the solid line indicates results using the analytical formula in Eq. 4.4	28
4.3	A qualitative illustration of the Gaussian pdfs in the marks and spaces. I_{th} is the optimal decision threshold current.	30

4.4	System setup of the XPM wavelength converter and its propagation. TX: Transmitter; EDFA: Erbium-doped fiber amplifier; SMF: Single mode fiber; DCF: Dispersion compensating fiber; HNL-DSF: High non-linearity dispersion shifted fiber; BPF: Band-pass filter; RX: Receiver sub-system.	34
4.5	Frequency spectra before propagation through the transmission system. The spectrum of the original signal is shown with a dashed line and that of the wavelength-converted signal is shown with a solid line.	38
4.6	The time sequence after wavelength conversion. The solid red curve is from the standard transmitter and the dashed blue curve is that of the wavelength-converted signal. The inset shows an isolated space.	39
4.7	The BER as a function of propagation distance. The solid line shows the BER for the wavelength-converted signal and the dashed line shows the BER for the standard 80-Gb/s signal.	40

LIST OF TABLES

3.1 Advantages and disadvantages of various wavelength conversion methods	23
---	----

1. INTRODUCTION

The need for high speed and reliable communication systems has led to the development of optical fibers. The discovery of glass as a viable alternative to copper cables, and the rapid research and development that resulted have revolutionized communications [1]. Optical fibers are better than copper, wireless or coaxial cables, in that they are more secure, since they cannot be tapped and are immune to interference from external sources. Though commercial fiber optic lines were deployed in the late seventies, it was only after the invention of the erbium doped fiber amplifier (EDFA) that high-speed and long-haul wavelength division multiplexed (WDM) systems gained prominence. Today, several terabytes per second can be transmitted over a single optical fiber [3].

The physics of optical fiber communication systems is now well understood, and their performance can be accurately calculated using computer aided modeling and simulation tools. Effects like fiber nonlinearity, polarization effects, noise due to optical amplifiers, and receiver effects are all included in modern-day computational tools. These design tools reduce the amount of experimentation that is needed to design systems, thus substantially reducing development costs.

For robust operation of high speed networks, wavelength conversion, as

well as new signal processing and coding techniques are important. All-optical wavelength conversion potentially plays an important role in enhancing the performance of future high speed and high capacity optical networks. The methods demonstrated to date utilize the ultra-fast Kerr nonlinearity in optical media. The principle of utilizing cross-phase modulation (XPM) in glass fibers has been successfully demonstrated by experimental groups [23, 24]. The basic idea of this technique is to modulate a continuous wave (CW) pump using the XPM interaction between the pump signal and a data signal. The induced phase modulation is then converted into an intensity modulation by optically filtering the pump wave. A tunable optical filter can be used to reject one of the sidebands or even the optical carrier. This method has been demonstrated experimentally to be scalable for data rates up to 160-Gb/s [24]. Small-signal models, which give approximate analytical expressions for some performance metrics [22, 26], have been used to model this system. However a study of the tolerance of the wavelength-converted signal to long-haul propagation in an optical communication system has yet to be reported. The purpose of the current work is to model the impact of long propagation lengths through fiber on XPM-induced wavelength conversion.

The thesis is organized as follows. Following this Introduction, Chapter 2 discusses the physical origin of the Kerr nonlinearity in optical fibers, and the impairments that it causes in high speed optical communication systems. Other nonlinear effects that appear in optical fibers, stimulated Raman scattering (SRS) and stimulated Brillouin scattering (SBS), are beyond the scope of this thesis. In chapter 3, I move on to the signal processing application of wavelength conversion. I discuss several wavelength conversion techniques.

Chapter 4 describes the use of XPM in highly-nonlinear, dispersion-shifted fiber (HNL-DSF) for wavelength conversion, the small signal model that has been developed for sinusoidal signals, the semi-analytical method for calculation of the bit error ratio (BER), and a propagation study of wavelength converted signals in a noise-limited communication system. I show that the BER of the wavelength-converted signal is almost the same as that of a standard 80-Gb/s signal after both signals have propagated through a 1000 km long transmission system, based on alternating spans of single-mode fiber (SMF) and dispersion compensating fiber (DCF). Apart from cleaning up phase noise in the incoming signal, wavelength conversion also improves the extinction ratio of the pulses. These results provide a motivation for the further development of in-line, fiber-based wavelength converters. I summarize the key findings, and conclude with chapter 5.

2. FIBER NONLINEARITIES

As long as the optical power within an optical fiber is small, the fiber can be treated as a linear medium. However when the power levels are in the order of tens of milliwatts, nonlinear effects become important, placing significant limitations on high-speed wavelength-division multiplexed (WDM) systems. Nonlinear effects can be classified into two categories: stimulated scattering (Raman and Brillouin scattering) in which optical energy is lost, and the Kerr effect that induces a nonlinear phase shift with no loss of energy. In this chapter, I describe the Kerr effect, which is the nonlinearity arising from the intensity dependence of the refractive index of the fiber [6]. The propagation of light in a non-magnetic dielectric medium like SiO₂ can be described by Maxwell's equation

$$\nabla^2 \mathbf{E}(\mathbf{r}, t) + \frac{1}{c^2} \frac{\partial^2 \mathbf{E}(\mathbf{r}, t)}{\partial t^2} + \mu_o \frac{\partial^2 \mathbf{P}(\mathbf{r}, t)}{\partial t^2} = 0, \quad (2.1)$$

where the vectors $\mathbf{E}(\mathbf{r}, t)$ and $\mathbf{P}(\mathbf{r}, t)$ are the electric field and the induced polarization field respectively, c is the velocity of light in vacuum, and μ_o is the permeability in free space. The induced polarization field $\mathbf{P}(\mathbf{r}, t)$ can be defined as the dipole moment per unit volume, resulting from the charge separation due to the applied electric field. The dependence of $\mathbf{P}(\mathbf{r}, t)$ on

$\mathbf{E}(\mathbf{r}, t)$ can be written as a Taylor expansion

$$\mathbf{P}(\mathbf{r}, t) = \epsilon_0 [\chi^{(1)} \cdot \mathbf{E}(\mathbf{r}, t) + \chi^{(2)} : \mathbf{E}(\mathbf{r}, t)\mathbf{E}(\mathbf{r}, t) + \chi^{(3)} : \mathbf{E}(\mathbf{r}, t)\mathbf{E}(\mathbf{r}, t)\mathbf{E}(\mathbf{r}, t) + \dots], \quad (2.2)$$

where $\chi^{(n)}$ is the n -th order component of the electric susceptibility of the medium. In glass, the second-order susceptibility $\chi^{(2)}$ is zero due to inversion symmetry. Also, the polarization vector $\mathbf{P}(\mathbf{r}, t)$ can be written as the sum of its linear and nonlinear terms [1]

$$\mathbf{P}(\mathbf{r}, t) = \mathbf{P}_L(\mathbf{r}, t) + \mathbf{P}_{NL}(\mathbf{r}, t), \quad (2.3)$$

where, dropping the higher order terms in Eq. (2.2), I define $\mathbf{P}_L(\mathbf{r}, t)$ and $\mathbf{P}_{NL}(\mathbf{r}, t)$ as

$$\begin{aligned} \mathbf{P}_L(\mathbf{r}, t) &= \epsilon_0 [\chi^{(1)} \cdot \mathbf{E}(\mathbf{r}, t)], \\ \mathbf{P}_{NL}(\mathbf{r}, t) &= \epsilon_0 [\chi^{(3)} : \mathbf{E}(\mathbf{r}, t)\mathbf{E}(\mathbf{r}, t)\mathbf{E}(\mathbf{r}, t)]. \end{aligned} \quad (2.4)$$

Because of this nonlinear term, silica exhibits a power-dependent variation of refractive index, known as the Kerr effect. The power-dependent refractive index can be written as [4]

$$n = n_o + \frac{3}{8n_o} \chi_r^{(3)} I = n_o + \bar{n}_2 I, \quad (2.5)$$

where $\chi_r^{(3)}$ is the real part of susceptibility, \bar{n}_2 is the nonlinear index coefficient (\bar{n}_2 is $2.6 \times 10^{-20} \text{ m}^2/\text{W}$ for silica fibers), and I is the optical intensity in the fiber. This change in the refractive index of the fiber results in a phase

change of

$$\phi_{\text{NL}} = \gamma |u(z, t)|^2 L_e. \quad (2.6)$$

Assuming that light is in a single polarization state, the field envelope $u(z, t)$ can be related to the electric field vector $\mathbf{E}(\mathbf{r}, t)$, the single-mode profile \mathbf{F} , and the propagation constant β by [8]

$$\mathbf{E}(\mathbf{r}, t) = \left[\frac{\omega_0}{2\epsilon_0 c^2 \beta(\omega_0)} \right]^{1/2} u(z, t) \mathbf{F}(x, y) \exp [i(\beta z - \omega_0 t)] + \text{c.c.} \quad (2.7)$$

The transverse modal field is normalized so that [7]

$$\int dx \int dy |\mathbf{F}(x, y)|^2 = 1, \quad (2.8)$$

where $\mathbf{F}(x, y)$ is a vector obtained by projecting \mathbf{F} onto the plane perpendicular to the propagating direction [7]. With this normalization, $|u(z, t)|^2$ equals the local power. The nonlinear coefficient γ and the effective nonlinear length of the fiber L_e are [4]

$$\begin{aligned} L_e &= \frac{1 - e^{-\alpha L}}{\alpha}, \\ \gamma &= \frac{2\pi \bar{n}_2}{\lambda A_{\text{eff}}}. \end{aligned} \quad (2.9)$$

The parameter A_{eff} denotes the effective core area and is [4]

$$A_{\text{eff}} = \frac{(\iint |\mathbf{F}(x, y)|^2 dx dy)^2}{\iint |\mathbf{F}(x, y)|^4 dx dy}. \quad (2.10)$$

In order for Eq. (2.6) to be valid, the dispersive scale length L_D should be short compared to the length of the fiber, L . For a pulse width of T_0 and a second-order dispersion parameter β_2 , one may express L_D as $L_D = T_0^2/|\beta_2|$. Herrera, *et al.* [26] choose $\beta_2 = 2.31 \times 10^{-28}$ s²/m and $L = 10$ km. Setting $T_0 = 25$ ps, which equals the modulation period, we find that $L_D = 2.71 \times 10^6$ m, so that $L \ll L_D$, and the effect of dispersion is negligible. In order to neglect polarization effects, the light should be in a single polarization state as a function of time at every point z along the fiber, although this polarization state may evolve as a function of z . Thus, the polarization states of the signal and pump must be aligned when they are launched into the fiber, and the polarization mode dispersion must be small over the length L and over the bandwidth of interest, which in the case of Rau, *et al.* [24] is the combined bandwidth of the signal and the pump, and is approximately 7 nm.

The phase change in Eq. (2.6) becomes significant when the product of power and the effective length of the system reaches 1 W-km. Even though the nonlinear index is small, the high power levels and lengths make it a significant factor in long-haul systems. Depending on whether the intensity modulation is due to the channel's own intensity or is due to the intensity of one or more of the co-propagating channels, the Kerr effect induces three nonlinear phenomena: self-phase modulation (SPM), cross-phase modulation (XPM), and four wave mixing (FWM).

2.1 Self-phase modulation

SPM is the dominant nonlinear phenomenon affecting the performance of single-channel lightwave systems. SPM gives rise to a time-dependent phase modulation of the optical signal, leading to spectral broadening. The SPM-induced time-dependent phase shift in each fiber span is given by [2]

$$\begin{aligned}\phi_{\text{SPM}}(z, t) &= \int_0^L \gamma P(z) dt, \\ \phi_{\text{SPM, max}} &= \gamma P_{\text{in}} L_e,\end{aligned}\tag{2.11}$$

where P_{in} is the peak input power and $P(z) = P_{\text{in}} \exp(-\alpha z)$. Here α is the fiber attenuation coefficient, and P_{in} is time dependent. If the transmission system has periodically spaced amplifiers, then the phase ϕ_{SPM} in Eq. (2.11) is multiplied by the number of amplifiers N_A . In order to keep the impact of SPM in the system at a reasonable level, one operates in the limit $\phi_{\text{SPM}} \ll 1$. SPM-induced spectral broadening is a consequence of the time dependence of $\phi_{\text{SPM}}(z, t)$. A temporally varying phase implies that the instantaneous optical frequency differs from its central value by [4]

$$\delta\omega(t) = \frac{\partial\phi_{\text{SPM}}}{\partial t} = \frac{\partial P_{\text{in}}}{\partial t} \gamma L_e.\tag{2.12}$$

The time dependence of $\delta\omega$ corresponds to a frequency chirp. As a signal pulse propagates along an optical fiber, this chirp grows, and new frequency components are generated, symmetrically broadening the signal spectrum around the carrier. The extent of spectral broadening depends on the initial pulse shape of the bits in the optical signal. In the time domain, the envelope

of each pulse is not changed; however, in any real medium the effects of dispersion will simultaneously act on each pulse. In regions of normal dispersion, the *red* portions of the pulse have a higher velocity than the *blue* portions, and thus the front of the pulse moves faster than the back, broadening the pulse in time. In regions of anomalous dispersion, the opposite is true, and the pulse is compressed temporally and becomes shorter.

2.2 Cross-phase modulation

The intensity-dependent nonlinear effects are quite pronounced in WDM systems because of XPM. In XPM, the modulation of the fiber refractive index is caused by power variations of adjacent channels. Similarly to SPM, XPM-induced phase modulations are partially converted to intensity distortions of the optical signal by chromatic dispersion. To understand the origin of XPM, consider a WDM system with two channels.

$$u(z, t) = u_1 \cos(\beta_1 z - \omega_1 t) + u_2 \cos(\beta_2 z - \omega_2 t). \quad (2.13)$$

Note that $\omega_{1,2}$ and $\beta_{1,2}$ denote respectively the frequency and propagation constant differences from the carrier frequency ω_0 and the propagation constant $\beta(\omega_0)$ at that frequency. Using Eq. (2.4) we can write the nonlinear

polarization as [2, 6]

$$\begin{aligned}
P_{\text{NL}}(z, t) &= \epsilon_0 \chi^{(3)} \left[u_1 \cos(\beta_1 z - \omega_1 t) + u_2 \cos(\beta_2 z - \omega_2 t) \right]^3 \\
&= \epsilon_0 \chi^{(3)} \left\{ \left(\frac{3u_1^3}{4} + \frac{3u_2^2 u_1}{2} \right) \cos(\beta_1 z - \omega_1 t) \right. \\
&\quad + \left(\frac{3u_2^3}{4} + \frac{3u_1^2 u_2}{2} \right) \cos(\beta_2 z - \omega_2 t) \\
&\quad + \frac{3u_1^2 u_2}{4} \cos[(2\beta_1 - \beta_2)z - (2\omega_1 - \omega_2)t] \\
&\quad + \frac{3u_2^2 u_1}{4} \cos[(2\beta_2 - \beta_1)z - (2\omega_2 - \omega_1)t] \\
&\quad + \frac{3u_1^2 u_2}{4} \cos[(2\beta_1 + \beta_2)z - (2\omega_1 + \omega_2)t] \\
&\quad + \frac{3u_2^2 u_1}{4} \cos[(2\beta_2 + \beta_1)z - (2\omega_2 + \omega_1)t] \\
&\quad + \frac{u_1^3}{4} \cos(3\beta_1 z - 3\omega_1 t) \\
&\quad \left. + \frac{u_2^3}{4} \cos(3\beta_2 z - 3\omega_2 t) \right\}. \tag{2.14}
\end{aligned}$$

The terms at $2\omega_1 + \omega_2$, $2\omega_2 + \omega_1$, $3\omega_1$, and $3\omega_2$ can be neglected since the phase-matching conditions will not be satisfied due to the presence of fiber chromatic dispersion [6], as follows from Eq. (2.21) in Sec. 2.3. The component of dielectric polarization at ω_1 can be written as

$$P_{\text{NL}}(\omega_1) = \frac{3}{4} \epsilon_0 \chi^{(3)} (u_1^2 + 2u_2^2) u_1 \cos(\beta_1 z - \omega_1 t). \tag{2.15}$$

In Eq. (2.15) the first term is due to SPM while the second term is due to XPM. We see that the phase of the sinusoidal term at ω_1 changes in proportion to u_2 and vice versa. Hence, the phase shift for a specific channel depends on the power of the other channels. The total phase shift for the i -th channel

can in general be written for N channels as [4]

$$\phi_i^{\text{NL}} = \frac{\gamma}{\alpha} \left(P_i + 2 \sum_{m \neq i}^N P_m \right). \quad (2.16)$$

This nonlinear phase shift depends on the bit pattern and the power in the different channels and can have a maximum value of $\phi_{\text{max}} = (\gamma/\alpha)(2N-1)P_i$, assuming equal power for all channels. The effects of XPM are negligible if there is no dispersion in the fiber. However, the phase fluctuations are converted to intensity fluctuations in the presence of dispersion and reduce the output signal to noise ratio (SNR). Based on the pump-probe model, the phase modulation in channel 1 induced by channel 2, due to XPM alone is [5]

$$\phi_{1,\text{XPM}}(L, t) = 2\gamma \int_0^L P_2(0, t + d_{12}z) \exp(-\alpha z) dz, \quad (2.17)$$

where $P_2(z, t)$ is the power of channel 2, γ is the nonlinear coefficient, α is the attenuation coefficient, L is the fiber length, $d_{12} = D\Delta\lambda$ is the relative walk-off between the two channels with wavelength separation $\Delta\lambda$, and D is the fiber dispersion coefficient.

2.3 Four-wave mixing

The beating between optical waves at different frequencies leads to energy exchange between them. We saw in Eq. (2.14) that the intensity dependence of refractive indices not only induces phase shifts within a channel and other channels, but also generates new frequencies. This phenomenon is called four-wave mixing (FWM). FWM is critically dependent on the channel spacing

and chromatic dispersion. Three frequency components f_i, f_j, f_k traveling through a fiber generate new spectral components at

$$f_{ijk} = f_i + f_j - f_k. \quad (2.18)$$

For distinct i, j, k , nine new frequencies are generated. SPM ($i = j = k$) and XPM ($i \neq j = k, i = j \neq k$), if the frequencies are not all distinct, can be considered special cases of FWM. The power of a generated component is [5]

$$P_{ijk} = \eta(\gamma LD/2)^2 P_i P_j P_k, \quad (2.19)$$

where P_i is the power of the i -th component and D is a degeneracy factor (equal to 1, 3, or 6 depending on whether 3, 2, or 0 spectral components are interacting). The parameter η is the FWM efficiency defined as [5]

$$\eta = \frac{\alpha^2}{\alpha^2 + \Delta\beta^2} \left\{ 1 + \frac{4 \exp(-\alpha L) \sin(\Delta\beta L/2)}{[1 - \exp(-\alpha L)]^2} \right\}. \quad (2.20)$$

The FWM efficiency η depends on the channel spacing through the phase mismatch given by

$$\Delta\beta(\omega) = \beta_{ijk} + \beta_k - \beta_i - \beta_j \approx \beta_2(\omega_0)(\omega_i - \omega_k)(\omega_j - \omega_k). \quad (2.21)$$

2.4 Propagation of light in optical fibers

Transmission of light in an optical fiber is described by an extended version of the nonlinear Schrödinger equation (NLSE)

$$i\frac{\partial u(z,t)}{\partial z} - \frac{1}{2}\beta''\frac{\partial^2 u(z,t)}{\partial t^2} - \frac{i}{6}\beta'''\frac{\partial^3 u(z,t)}{\partial t^3} + \gamma|u(z,t)|^2u(z,t) - i\alpha u(z,t) = 0, \quad (2.22)$$

where $u(z,t)$ is the optical field, β'' is the local dispersion, β''' is the dispersion slope, γ is the nonlinear coefficient and α is the loss coefficient of the fiber. The solution to this nonlinear partial differential equation cannot be expressed analytically with arbitrary initial conditions. A number of numerical methods have been proposed to study the effect of nonlinearity in optical fibers by solving Eq. (2.22). The split-step Fourier method is one of them, and is the most commonly used. For a given step size Δz the various steps in the symmetric split-step Fourier algorithm can be written as

$$\begin{aligned} u_{D1}(\omega) &= u(z,\omega) \exp \left[\left(\frac{i}{2}\beta''\omega^2 + \frac{i}{6}\beta'''\omega^3 \right) \frac{\Delta z}{2} \right], \\ u_{D1}(t) &= \text{IFFT}[u_{D1}(\omega)], \\ u_{NL}(t) &= u_{D1}(t) \exp(i\gamma|u_{D1}(t)|^2\Delta z), \\ u_{NL}(\omega) &= \text{FFT}[u_{NL}(t)], \\ u(z+\Delta z,\omega) &= u_{NL}(\omega) \exp \left[\left(\frac{i}{2}\beta''\omega^2 + \frac{i}{6}\beta'''\omega^3 \right) \frac{\Delta z}{2} \right], \\ u(z+\Delta z,t) &= \text{IFFT}[u(z+\Delta z,\omega)], \end{aligned} \quad (2.23)$$

where $\text{FFT}\{\cdot\}$ and $\text{IFFT}\{\cdot\}$ refer to the forward and inverse fast-Fourier transform operations respectively. There are different algorithms for choosing

efficient step sizes while modeling the propagation of light in fibers [9]. The widely used *constant step-size method* uses constant step sizes, while the *logarithmic step-size method* employs a logarithmic distribution of the step sizes. In the *nonlinear phase rotation method*, the step size is chosen so that the phase change due to nonlinearity does not exceed a specified limit. In the *walk-off method*, the step size is chosen to be inversely proportional to the product of the absolute value of dispersion and the spectral bandwidth of the signal. My simulations employ the *relative-error method* for choosing step sizes, which is an adaptive method for setting the step size using a measure of the local error, since this method performs well over a wide range of parameters and systems [9].

3. WAVELENGTH CONVERSION

The available bandwidth in optical fibers is several terahertz. To utilize the full potential of future high-speed networks, efficient signal switching and routing methods are necessary. Wavelength converters are devices used in WDM networks to convert an incoming signal at one wavelength to another. They are needed for three major reasons.

- A signal may enter a network at a wavelength that is not in use in that network. For instance, first generation networks using LEDs or Fabry-Perot lasers transmit data in the 1310 nm window. This wavelength is not compatible with modern WDM systems. Hence, these signals must be converted to narrow-band WDM signals in the 1550 nm range using wavelength converters called transponders [2].
- Wavelength converters are needed to improve the wavelength utilization in a network through wavelength reuse [10].
- Wavelength converters are needed at the boundaries between two networks managed by different entities using different wavelength management protocols [11].

Three wavelength conversion techniques will be discussed in this section: optoelectronic regeneration, optical gating, and wave mixing.

3.1 Optoelectronic regeneration

Optoelectronic regeneration is the simplest approach to wavelength conversion. The input signal is first detected; it is then regenerated and is used to drive a laser at the required wavelength. A tunable laser is used to create a variable wavelength output. There are three types of regeneration possible [2].

In 1R regeneration (re-amplification without reshaping), the receiver system converts the signal into electrical form; it is then amplified and is used to drive the laser. This form is transparent to the data format, but it adds noise through amplifier spontaneous emission (ASE). The block diagram of the 1R regeneration method is shown in Fig. 3.1(a).

The second type of regeneration is 2R regeneration (re-amplification with reshaping), where the signal is reshaped by passing it through a logic gate [2, 12]. This approach can only be used with digital data formats, and it adds additional phase jitter. Several all-optical 2R regenerators have previously been demonstrated with optoelectronic devices like semiconductor optical amplifiers (SOAs), a semiconductor optical amplifier-Mach-Zehnder interferometer (SOA-MZI) combination [13], and Q -switched lasers [14]. Their cascadability is however limited by jitter accumulation [12]. The block diagram of 2R regeneration is shown in Fig. 3.1(b).

The last alternative is 3R regeneration, i.e., re-amplification with reshaping and retiming [16]. A block diagram of 3R regeneration is shown in Fig. 3.1(c). This approach is complete in the sense that it compensates for the effect of fiber chromatic dispersion and nonlinearity. Since retiming is a process that depends on the bit rate and modulation format, transparency is

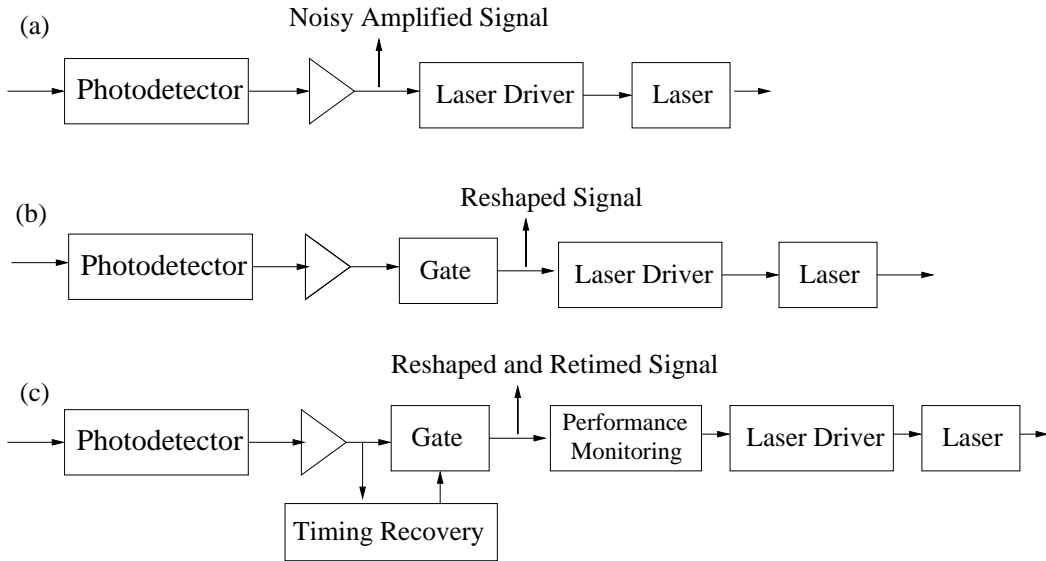


Fig. 3.1: Schematic of the three types of opto-electronic regeneration: (a) 1R: re-amplification, (b) 2R : re-amplification and reshaping, and (c) 3R: re-amplification, reshaping, and retiming. Reproduced from [2].

lost. The circuits used are typically complex, involving timing recovery and performance monitoring circuitry. To achieve 3R regeneration, many optical clock recovery methods have been studied and validated in transmission experiments [15].

3.2 Optical gating techniques

Optical gating techniques employ devices like semiconductor optical amplifiers, whose gain characteristics change with the intensity of an input signal, due to gain saturation. These types of converters are preferred over opto-electronic methods because of their low cost and simple packaging. There are many wavelength conversion methods that fall into this category be-

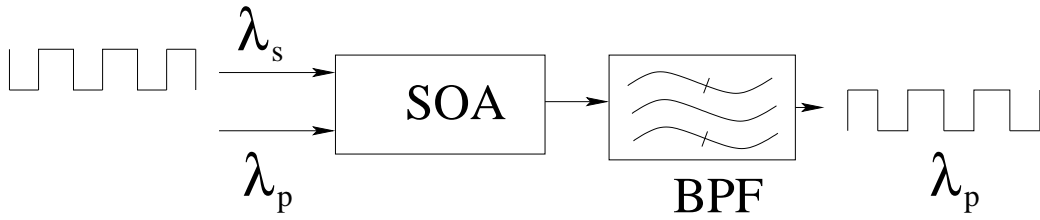


Fig. 3.2: Schematic of the wavelength conversion technique utilizing cross-gain modulation in semiconductor optical amplifiers.

cause there are numerous optical gating mechanisms available. This category includes cross-gain modulation (XGM) in semiconductor optical amplifiers (SOAs), cross-phase modulation (XPM) in SOAs, and nonlinear optical loop mirrors.

The principle involved in utilizing SOAs for wavelength conversion is cross-gain modulation (XGM), a nonlinear effect in SOAs [18]. XGM makes use of the gain dependence of an SOA on its input intensity. As the optical power increases, the gain of an SOA saturates due to carrier depletion [1]. Therefore, it is possible to modulate the amplifier gain with an input signal, and then encode this gain modulation on a separate continuous wave (CW) probe traveling through the amplifier at another wavelength. Figure 3.2 illustrates the principle of XGM in SOA. The CW input at wavelength λ_p is not amplified when the information signal is high (mark), and is amplified when the information signal is zero (space). This physical operation maps the signal from λ_s to λ_p , with logic inversion [17]. A band-pass filter at the output isolates the target wavelength. Wavelength converters based on XGM have limited cascadability, owing to degradation of the signal extinction ratio [19] and SNR degradation due to ASE noise. The high signal power can

further affect the phase of the probe and distort the output [2]. Despite these shortcomings, XGM is popular due to its simplicity and conversion efficiency.

Another gating technique uses nonlinear optical loop mirrors (NOLMs) [20]. The NOLM consists of a loop of fiber with a 3 dB coupler, which allows the pump at the target wavelength to split and travel around the loop in opposite directions. In the absence of a signal that interacts with the pump, the pump is in phase after one round trip and only exits the loop through the in-phase port of the 3-dB coupler. The signal is coupled into and out of the loop in only one direction. The signal overlaps with the pump traveling in one direction for a certain distance, so that the pump travelling in that direction experiences a phase shift due to the nonlinear interaction, relative to the pump travelling in the other direction. This relative phase changes the coupling, and the modulated pump couples out of the quadrature port of the 3-dB coupler.

3.3 Wave-mixing techniques

Wave mixing is a nonlinear effect that is present in nonlinear optical materials and that produces new frequencies as described in Sec. 2.3. Typical converters using this technique are based on difference frequency generation and FWM in waveguides and SOAs. We saw earlier in Sec. 2.2 that the phase and frequencies of the generated wave is dependent on the frequencies of the interacting waves. This method of wavelength conversion is the only one that has strict modulation format and bit-rate transparency [10, 11], meaning that they could be used with different data formats. However with high-

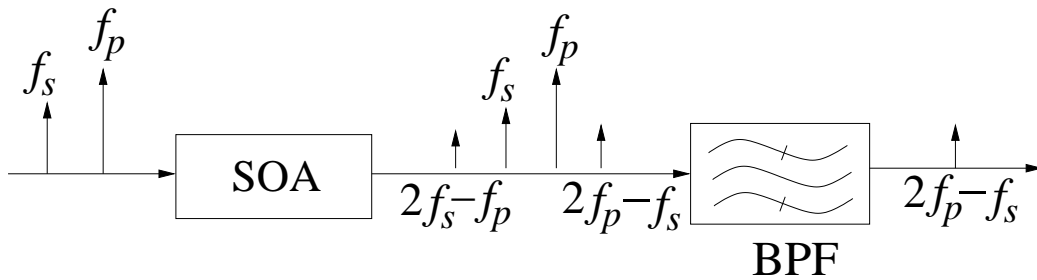


Fig. 3.3: Schematic of a wavelength converter utilizing four-wave mixing in a semiconductor optical amplifier.

speed communication systems, maintaining the full-width at half maximum (FWHM) of the pulses in the data-stream is an issue when utilizing nonlinear conversion techniques. Three-wave mixing is a second-order optical effect, while four-wave mixing is a third-order process. FWM is a low-efficiency process, in which the typical converted power is 15-20 dB lower than the input signal power [10]. The four-wave mixing power can be increased by using an SOA instead of a waveguide, because of the high intensities inside an SOA. This phenomenon is illustrated in Fig. 3.3. If the signal and the pump are at frequencies f_s and f_p , FWM produces waves at $2f_s - f_p$ and $2f_p - f_s$ as long as the frequencies are within the amplifier bandwidth. The required frequency component is then filtered out.

Among wave-mixing devices, optical parametric amplifiers (OPA) can be used as parametric wavelength converters. They use the interaction of three optical frequencies through the second-order nonlinearity of the material [21]. The frequency relationships are governed by energy and momentum conservation equations. OPAs can be continuously tuned by turning the angle of the crystal or by varying the temperature. Lithium niobate (LiNbO_3) was

the earliest nonlinear material used for parametric conversion.

3.4 Fiber-based wavelength conversion

Wavelength conversion has been demonstrated experimentally using XPM in both high-nonlinearity, dispersion-shifted fibers (HNL-DSF) [23, 24], as well as in normal dispersion holey fibers [25]. This section describes the experimental method employed by Rau, et al. [24] for demonstrating phase-noise cleaning, all-optical wavelength conversion at 160-Gb/s using HNL-DSF. The experimental setup is shown in Fig. 3.4. They employ a passive multiplexer to combine sixteen 10-Gb/s channels at 1554.5 nm and a pulse FWHM of 1.5 ps. The CW signal is at 1547 nm, which is sufficiently far from the zero-dispersion wavelength of the HNL-DSF to avoid generating spurious FWM components that are prone to evolve around the zero dispersion wavelength, as seen in section 2.3. The 160-Gb/s OTDM data was then combined with the CW signal, amplified using an EDFA and injected into the fiber. Rau, et al. [24] found that the CW signal power has to be lower than the data signal power, to maintain a good SNR at the output. As explained in earlier sections, the data signal modulates the CW signal, thereby generating side tones due to phase modulation. The approximate bandwidth of the generated sidetones can be obtained from Eq. (2.17) by using the relation $\delta\omega \sim |\partial\phi_{\text{XPM}}/\partial t|$. A filter that is offset in frequency by 160 GHz from the CW frequency is used to filter out one of the side tones. This filtering produces amplitude modulation in addition to the phase modulation, thereby yielding the wavelength-converted signal.

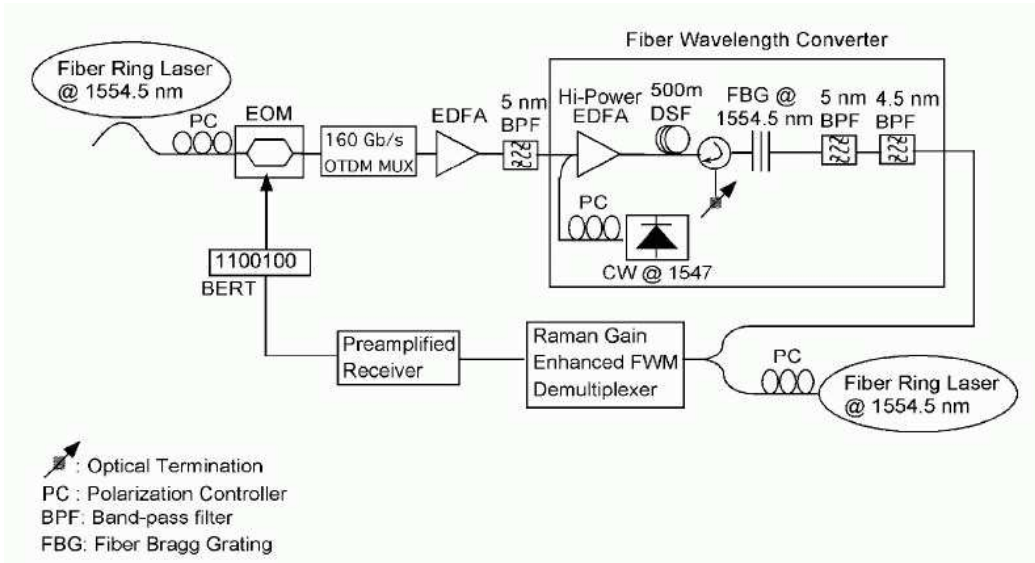


Fig. 3.4: Experimental setup of the all-optical wavelength converter showing the MUX-DEMUX links. Reproduced from [24].

The pulses generated in the fiber-ring laser used in the experiments suffer from poor phase correlation, and therefore do not exhibit well-defined frequency tones. However, the wavelength-converted signal has well-defined tones, showing that wavelength conversion improves the signal. The digital performance of the system was then measured by demultiplexing the 16 channels, and detecting each channel using a pre-amplified receiver. All the channels had a BER of $< 10^{-9}$.

Table 3.1 lists the advantages and disadvantages of the wavelength conversion techniques discussed in this chapter. Wave-mixing converters are the only type of converters offering transparency. But they suffer from low conversion efficiency, as well as a narrow bandwidth. The SOA-based converters provide an alternative to costly optoelectronic regenerators, but they suffer from SNR degradation. The XPM-based fiber converter that we discussed

Tab. 3.1: Advantages and disadvantages of various wavelength conversion methods

Method	Advantages	Disadvantages
Optoelectronic	Ready to deploy Pulse retiming and re-shaping is possible	Cost scales up with bit-rate Limited cascadability due to jitter accumulation
Gating	Simple packaging Gain in converted signal	High SNR degradation, noise and chirp Limited cascadability
Wave-mixing	Bit-rate and format transparency Chirp reversal is possible	Narrow conversion bandwidth Low conversion efficiency

last offers bit-format and bit-rate transparency. Such all-optical wavelength converters are needed in modern networks, so that users are not limited to a specific bit rate or modulation format, and to enable future upgrades.

4. WAVELENGTH CONVERSION USING CROSS-PHASE MODULATION

The use of XPM in glass fibers for wavelength conversion has been successfully demonstrated in laboratory experiments [23]. This method has been demonstrated for data rates up to 160 Gb/s [23, 24]. The method devised in [23] is to combine an incoming data-modulated signal at one wavelength with a continuous wave (CW) signal at the desired output wavelength, and to propagate this combined signal through a short highly nonlinear dispersion-shifted fiber (HNL-DSF). XPM in the HNL-DSF then imposes a phase modulation onto the CW signal from the incoming data-modulated signal, generating optical sidebands. When the original CW carrier is suppressed by an optical filter, the phase modulation is converted to amplitude modulation, thereby generating the wavelength-converted data-modulated signal. Numerical simulations based on a small-signal analysis have shown that the technique has a high conversion efficiency [26], and wavelength shifts of up to 7 nm have been experimentally demonstrated [24].

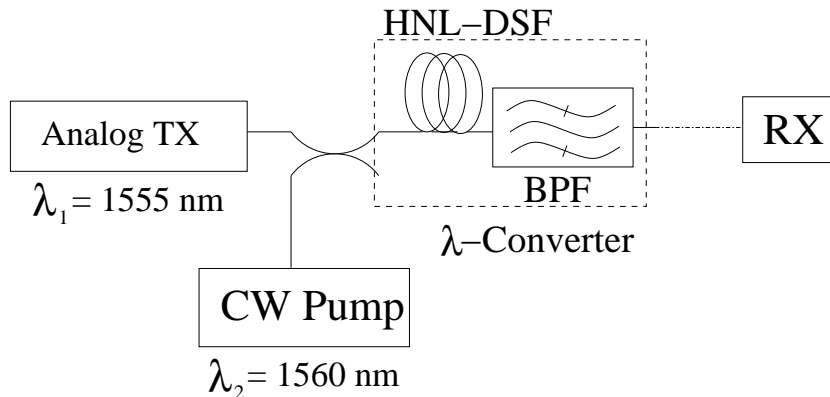


Fig. 4.1: Simulation setup for the small-signal model

4.1 Small-signal model

Small-signal models have been devised for wavelength conversion utilizing cross-gain modulation (XGM) in semiconductor optical amplifiers (SOAs) [22] and XPM in HNL-DSFs [26]. In [26] an expression for the conversion efficiency of analog optical signals is derived. In this section, I compare the results obtained using the small-signal model [26] to a numerical simulation using the split-step Fourier method. The scheme for the HNL-DSF based wavelength converter is shown in Fig. 4.1.

The propagation equations for the signal A_1 and the pump wave A_2 is written as [26]

$$\begin{aligned} \frac{\partial A_1}{\partial z} + \frac{\alpha}{2}A_1 + \beta_1' \frac{\partial A_1}{\partial t} - \frac{i}{2}\beta_1'' \frac{\partial^2 A_1}{\partial t^2} - \frac{1}{6}\beta_1''' \frac{\partial^3 A_1}{\partial t^3} &= -i\gamma(|A_1|^2 + 2|A_2|^2)A_1, \\ \frac{\partial A_2}{\partial z} + \frac{\alpha}{2}A_2 + \beta_2' \frac{\partial A_2}{\partial t} - \frac{i}{2}\beta_2'' \frac{\partial^2 A_2}{\partial t^2} - \frac{1}{6}\beta_2''' \frac{\partial^3 A_2}{\partial t^3} &= -i\gamma(2|A_1|^2 + |A_2|^2)A_2, \end{aligned} \quad (4.1)$$

where γ is the fiber nonlinear parameter, α is the attenuation; β' , β'' , and β'''

are the group-velocity, group-velocity dispersion and group-velocity dispersion slope respectively. We will consider a sinusoidal signal with sidebands, and a CW pump wave, so that

$$\begin{aligned} A_1(0, t) &= [P_S(1 + m_i \cos \Omega t)]^{1/2}, \\ A_2(0, t) &= \sqrt{P_P}, \end{aligned} \quad (4.2)$$

where P_S and P_P are the signal and pump powers respectively, m_i is the modulation index, and Ω is the frequency. Assuming that the signal power is much smaller than the pump power, and introducing the retarded distance and time $\xi = z$, $\tau = t - \beta'_2 z$, we can linearize Eq. (4.1). After further simplification by dropping the first- and second-order dispersion terms in Eq. (4.1), the pump power A_2 after propagation for a certain distance ξ can be written as

$$\begin{aligned} A_2(\xi, \tau) &= \sqrt{P_P} \exp(-\alpha\xi/2) \exp \left[-2i\gamma P_S \left(\frac{1 - \exp(-\alpha\xi)}{\alpha} \right) \right] \\ &\quad \exp \left(\frac{-2j\gamma P_S m_i}{\alpha^2 + \Omega^2(\Delta\beta)^2} \left\{ \exp(-\alpha\xi) \Omega(\Delta\beta) \sin \left[\Omega(\tau + \xi\Delta\beta) \right] \right. \right. \\ &\quad \left. \left. - \alpha \exp(-\alpha\xi) \cos \left[\Omega(\tau + \xi\Delta\beta) \right] \right. \right. \\ &\quad \left. \left. + \alpha \cos(\Omega\tau) - \Omega(\Delta\beta) \sin \Omega\tau \right\} \right), \end{aligned} \quad (4.3)$$

where I define $\Delta\beta = \beta'_1 - \beta'_2$. Equation (4.3) shows phase modulation of the pump wave by the signal intensity P_S . Applying the small signal approximation to the phase term of the pump wave [22], and using a linear approximation of the exponential terms, a small signal expression is obtained.

If we denote the sideband rejection ratio of the band-pass filter by ρ , and we define the wavelength conversion efficiency as the ratio between the photocurrent of the wavelength converted signal and the photocurrent of the original signal, the conversion efficiency may be written as [26]

$$\eta = \left| 2\gamma P_P (1 - 10^{-\rho/10}) \frac{\left\{ 1 - \exp \left[- (\alpha + j\Omega\Delta\beta) z \right] \right\} \exp(-\alpha z)}{\alpha + j\Omega\Delta\beta} \right|. \quad (4.4)$$

From Eq. (4.4), we infer that the efficiency has a linear dependence on the pump power and the fiber nonlinear parameter. The conversion efficiency described in Eq. (4.4) is compared with simulation results, where the propagation has been modeled using the split-step Fourier method. For this comparison I use a HNL-DSF with $\gamma = 16.7 \text{ W}^{-1}/\text{km}$, $\alpha = 0.72 \text{ dB}/\text{km}$ and a dispersion slope of $0.018 \text{ ps}/\text{nm}^2\text{-km}$. The signal and pump wavelength used are 1560 nm and 1555 nm respectively. The modulation frequency $\Omega = 40 \text{ GHz}$ and the signal power is 0 dBm . The modulation index m_i used in the simulations was 4% . Figure 4.1 shows the conversion efficiency as a function of the DSF length for different pump powers. The solid line indicates the plot obtained using Eq. (4.4), while the circles indicate the results obtained using the split-step Fourier method. The plot shows that the analytical expression gives a good approximation of the wavelength conversion efficiency. However, there is a slight deviation at higher powers and longer lengths, because Eq. (4.4) neglects dispersion [26]. This comparison also validates my code for solving the NLSE using the split-step Fourier method.

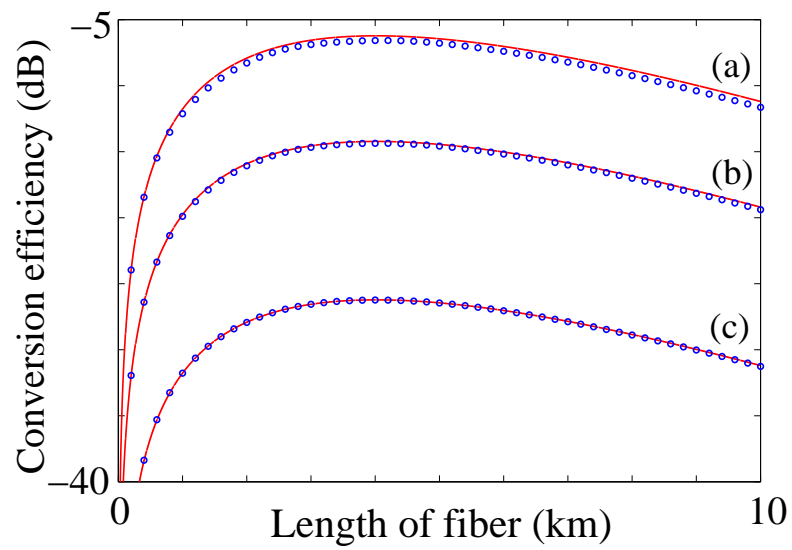


Fig. 4.2: Conversion efficiency as a function of fiber distance for varying pump powers (a) 10 dBm, (b) 6 dBm, and (c) 0 dBm. The circles indicates results obtained using the split-step Fourier method, while the solid line indicates results using the analytical formula in Eq. 4.4

4.2 Calculation of the bit-error ratio

The bit-error ratio (BER) is the fundamental measure of performance in optical fiber communication systems. The Q -factor is another widely used performance measure that is a function of the means and standard deviations of the electric currents in the marks and spaces. Assuming that the currents in the marks and spaces at the receiver are Gaussian distributed, the Q -factor can give a good estimate of the BER [27]. In practice, one often defines the Q -factor as a function of the BER. In that case, it is not really an independent performance measure.

The receiver makes a decision as to whether a mark or a space was transmitted by sampling the photocurrent. Because of the presence of noise, the bits could be detected erroneously. Let I_1 and I_0 be the mean currents at the marks and spaces respectively, and let σ_1 and σ_0 be the corresponding standard deviations. The Q -factor is defined as [1]

$$Q = \frac{I_1 - I_0}{\sigma_1 + \sigma_0}. \quad (4.5)$$

The decision circuit samples the bit and calls it a 1 if $I > I_{\text{th}}$ and a 0 if $I < I_{\text{th}}$. The choice of I_{th} should minimize the BER. Figure 4.3 shows the probability density functions of the observed photocurrent and the location of the optimal decision threshold. If the probability of receiving a mark and a space are $p(1)$ and $p(0)$ respectively, the BER can be defined as [1]

$$\text{BER} = p(0)P(1|0) + p(1)P(0|1), \quad (4.6)$$

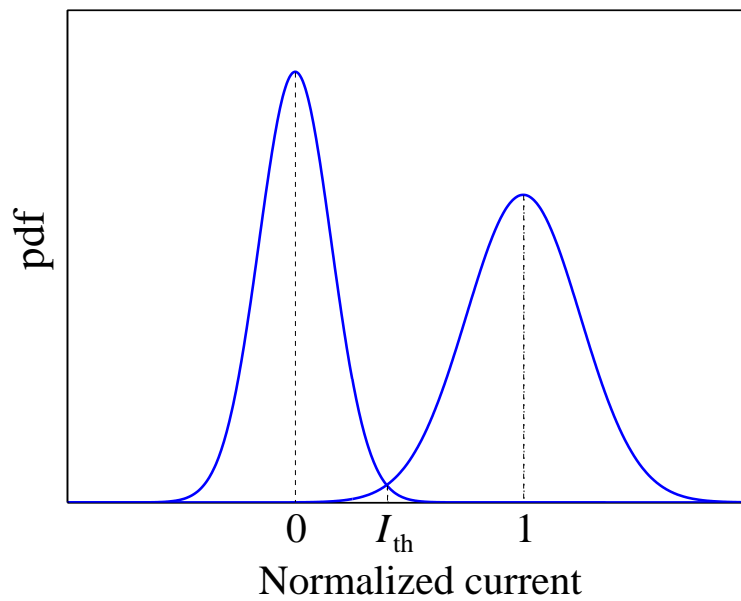


Fig. 4.3: A qualitative illustration of the Gaussian pdfs in the marks and spaces. I_{th} is the optimal decision threshold current.

where $P(1|0)$ is the conditional probability of erroneously deciding a 0 to be a 1 and $P(0|1)$ is the conditional probability of erroneously deciding a 1 to be a 0. Figure 4.3 shows a qualitative plot of the pdfs in the marks and spaces, and the optimal decision threshold based on the above approach. Assuming that an equal number of 1s and 0s is transmitted, the BER may be written as

$$\text{BER} = \frac{1}{2}[P(1|0) + P(0|1)]. \quad (4.7)$$

The conditional probabilities may be written as [1]

$$\begin{aligned}
P(1|0) &= \frac{1}{\sigma_0\sqrt{2\pi}} \int_{I_{\text{th}}}^{-\infty} \exp\left[-\frac{(I - I_0)^2}{2\sigma_0^2}\right] dI, \\
P(0|1) &= \frac{1}{\sigma_1\sqrt{2\pi}} \int_{-\infty}^{I_{\text{th}}} \exp\left[-\frac{(I - I_1)^2}{2\sigma_1^2}\right] dI.
\end{aligned} \tag{4.8}$$

Defining the complimentary error function $\text{erfc}(x)$ to be

$$\text{erfc}(x) = \frac{2}{\sqrt{\pi}} \int_x^{\infty} \exp(-y^2) dy, \tag{4.9}$$

the BER may be expressed as

$$\text{BER} = \frac{1}{4} \left[\text{erfc}\left(\frac{I_1 - I_{\text{th}}}{\sigma_1\sqrt{2}}\right) + \text{erfc}\left(\frac{I_{\text{th}} - I_0}{\sigma_0\sqrt{2}}\right) \right]. \tag{4.10}$$

Assuming that I_{th} is optimized to obtain a minimum BER, it can be related to the Q -factor using the relationship

$$\text{BER} = \frac{1}{2} \text{erfc}\left(\frac{Q}{\sqrt{2}}\right), \tag{4.11}$$

when $Q \gg 1$. In most experimental studies in which the Q -factor is reported, it is the BER that is measured and then Eq. (4.11) is used to obtain Q .

4.3 The semi-analytical receiver model

This section describes the receiver model that was used in my simulations and the performance measures. The BER and the Q -factor can be calculated from Eqs. (4.10) and (4.11) for multiple realizations of the transmission experiments using Monte-Carlo simulations. However to reduce the compu-

tational cost and time, I use the semi-analytical receiver model devised by Lima, et al. [28] to calculate the Q -factor.

The Lima, et al. [28] receiver model consists of an optical filter with a transfer function $H_o(\omega)$ and corresponding impulse response $h_o(t)$, a square-law photodetector with responsivity R and an electric filter with transfer function $H_e(\omega)$ and corresponding impulse response $h_e(t)$. The total electric current at the detection point is then given by

$$i(t) = R \left| [e_s(t) + e_n(t)] * h_o(t) \right|^2 * h_e(t), \quad (4.12)$$

where $e_s(t)$ and $e_n(t)$ denote the electric field envelopes of the signal and noise respectively, and $*$ denotes the convolution of two functions defined as

$$g(t) * h(t) = \int_{-\infty}^{\infty} g(\tau) h(t - \tau) d\tau. \quad (4.13)$$

Using Eq. (4.12) as the starting point, one may then derive the Q -factor, which Lima, et al. [28] show to be written as (Eq. 35 of [28])

$$Q = \frac{[i_s(t_1) + \langle i_n \rangle] - [i_s(t_0) + \langle i_n \rangle]}{\sqrt{[\sigma_{S-ASE}^2(t_1) + \sigma_{ASE-ASE}^2]} + \sqrt{[\sigma_{S-ASE}^2(t_0) + \sigma_{ASE-ASE}^2]}}, \quad (4.14)$$

where t_1 and t_0 are the sampling times of the highest mark and lowest space respectively, and the time-independent mean noise current is

$$\langle i_n \rangle(t) = \langle i_n \rangle = RN_{ASE}B_0. \quad (4.15)$$

The parameter $B_o=r_o(0)=\int_{-\infty}^{\infty} |h_o(\tau)|^2 d\tau$ is the noise equivalent bandwidth of the optical filter and N_{ASE} is the total noise power spectral density prior to the receiver. The terms $\sigma_{\text{S-ASE}}^2(t)$ and $\sigma_{\text{ASE-ASE}}^2$ in Eq. (4.14) are the variances of the current due to signal-noise beating and noise-noise beating respectively. These quantities may be defined as [28]

$$\begin{aligned}\sigma_{\text{S-ASE}}^2(t) &= R^2 N_{\text{ASE}} \Gamma_{\text{S-ASE}} I_{\text{S-ASE}}(t), \\ \sigma_{\text{ASE-ASE}}^2 &= \frac{1}{2} R^2 N_{\text{ASE}}^2 \frac{I_{\text{ASE-ASE}}}{\Gamma_{\text{ASE-ASE}}},\end{aligned}\quad (4.16)$$

where $I_{\text{S-ASE}}(t)$ and $I_{\text{ASE-ASE}}$ are the currents due to signal-noise beating and noise-noise beating respectively, as defined in Eqs. (26) and (29) of [28]. The term $\Gamma_{\text{ASE-ASE}}$ is called the noise-noise beating factor, and is the ratio between the variance of the current due to noise-noise beating if the noise were unpolarized to the actual variance of the current due to noise-noise beating. The term $\Gamma_{\text{S-ASE}}$ is called the signal-noise beating factor, and is the fraction of the noise that beats with the signal. These terms are defined in Eqs. (25) and (33) of [28]. These beating factors have a range of $1/2 \leq \Gamma_{\text{ASE-ASE}} \leq 1$ and $0 \leq \Gamma_{\text{S-ASE}} \leq 1$ respectively. For the case of unpolarized noise that I deal with in my studies, $\Gamma_{\text{ASE-ASE}} = 1$ and $\Gamma_{\text{S-ASE}} = 1/2$. Once the Q -factor is calculated using Eq. (4.14), the BER can be obtained using Eq. (4.11).

4.4 Simulation setup

Numerical simulations based on a small-signal analysis [26] have been discussed in Sec. 4.1, and large wavelength shifts have been experimentally

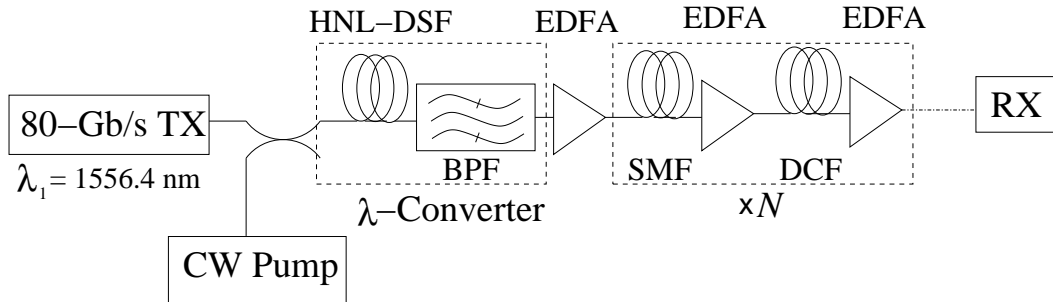


Fig. 4.4: System setup of the XPM wavelength converter and its propagation. TX: Transmitter; EDFA: Erbium-doped fiber amplifier; SMF: Single mode fiber; DCF: Dispersion compensating fiber; HNL-DSF: High non-linearity dispersion shifted fiber; BPF: Band-pass filter; RX: Receiver sub-system.

demonstrated [24] based on XPM in HNL-DSFs. However a study of the tolerance of the wavelength-converted signal to long-haul propagation in an optical communication system has yet to be reported. In this section, I describe a simulation study of a wavelength-converted signal at 80-Gb/s that is propagated over 1280 km, which consists of 16 transmission spans of 80 km length each. We find that the bit error ratio (BER) is comparable to that of a signal generated at the same wavelength by a standard transmitter.

The setup used for the simulation of wavelength conversion is shown in Fig. 4.4. The 80-Gb/s transmitter operates at a wavelength of 1556.4 nm and generates a return-to-zero (RZ) Gaussian format with a 16 bit pseudo-random binary data sequence. The pulses have an optical extinction ratio of 20 dB and full-width half maximum (FWHM) of 3 ps. The resulting signal simulates a single channel obtained by time-domain multiplexing eight 10-Gb/s signals using a passive multiplexer [24]. This data stream is combined with a CW pump at 1548.6 nm before being launched into a 1-km length of

HNL-DSF. The transmitter used in the simulations generates highly coherent pulses unlike the transmitter in the experiments, where amplitude distortion is observed due to poor phase correlation. Hence phase clean-up is not studied in the current simulations.

The CW power is 3 dBm and the average signal power is set to 20 dBm. The HNL-DSF has a zero dispersion wavelength of 1565 nm, a dispersion slope of 0.03 ps/nm²-km, and a nonlinear coefficient of 16.9 W⁻¹ km⁻¹. The parameters for the DSF were chosen from the fiber used in the small signal model analysis [26]. The short length of this highly nonlinear fiber reduces the dispersive walk-off. The high nonlinearity also reduces the power requirement. The data-modulated signal imposes phase modulation on the CW signal and generates sidebands. To suppress the CW signal, we use a third order supergaussian filter with 320 GHz bandwidth, centered with an optimal frequency offset of 160 GHz from the original CW signal. The transfer function $H(f)$ of a supergaussian filter is

$$H(f) = \exp \left[\frac{-(f - f_c)^{2n}}{2\sigma} \right], \quad (4.17)$$

where n is the order of the supergaussian filter, f_c is the center frequency of the filter, and σ is a width parameter related to the FWHM by

$$\sigma = \frac{1}{2} \frac{\text{FWHM}}{(\ln 2)^{1/2n}}. \quad (4.18)$$

We compare the performance of the wavelength-converted signal to that of a signal centered at a wavelength of 1548.6 nm that is generated by the

same 80-Gb/s transmitter described above. We will refer to this signal as the standard 80-Gb/s signal.

Both the standard 80-Gb/s signal and the wavelength-converted signal are propagated through a transmission system consisting of alternating spans of single mode fiber (SMF) and dispersion compensating fiber (DCF) and optical amplifiers. Since the converted signal is at a very low power, it is first pre-amplified to 3 dBm. The average power of the standard 80-Gb/s signal was also set to 3 dBm. Each of the transmission spans consists of 80 km of SMF with 16.7 ps/nm-km dispersion and DCF with -97.92 ps/nm-km dispersion that fully compensates the accumulated dispersion of the SMF. In addition erbium-doped fiber amplifiers (EDFAs) that compensate for the losses in the fibers, are present. The SMF and DCF have loss coefficients of 0.2 dB/km and 0.5 dB/km, respectively. The peak power during transmission is maintained at 2 mW by adjusting the gain of the EDFAs. The EDFAs add random amplifier spontaneous emission (ASE) noise, which has been modeled as additive white Gaussian noise (AWGN). The spontaneous emission factor n_{sp} of all EDFAs has been set to 1.28. The noise power at the end of each EDFA is given by

$$P_n = n_{\text{sp}} h\nu (G - 1) B_0, \quad (4.19)$$

where $h\nu$ is the photon energy, G is the linear gain of the EDFA and B_0 is the optical bandwidth. The frequency-converted signal is then passed through a receiver sub-system consisting of an optical filter, a square law photodetector and an electrical filter. The electrical filter is a fifth-order Bessel filter with a bandwidth of 80 GHz. The optical and electrical filter bandwidths have been

optimized to minimize the BER.

4.5 Setting up the computational window

Our computer simulations are based on the split-step fast Fourier transform (FFT) method. The frequency spectrum is discretized in powers of 2, since the FFT operates fastest when that is done. The CW frequency is chosen to be on the frequency grid and almost 7 nm away from the signal wavelength, as in the experiments [24]. The CW frequency must also be chosen so that it is well within the bandwidth of the simulation's frequency spectrum. As a rule of thumb, in calculations involving discrete transforms we need to set the number of samples N_0 , the resolution in the time domain ΔT , the time window T , and the frequency resolution ΔF so that

$$F_s \geq 2B, \quad (4.20)$$

where F_s is the sampling frequency, and B is the signal bandwidth. The parameters T , ΔF , and ΔT are thus

$$T = \frac{1}{F_s}, \quad \Delta F = \frac{1}{T}, \quad \text{and} \quad \Delta T = \frac{T}{N_0}. \quad (4.21)$$

4.6 Results and analysis

We now compare the transmission performance of the wavelength-converted signal to that of the standard 80-Gb/s signal. In Fig. 4.5, we show the frequency spectrum of the original 80-Gb/s signal before wavelength conversion

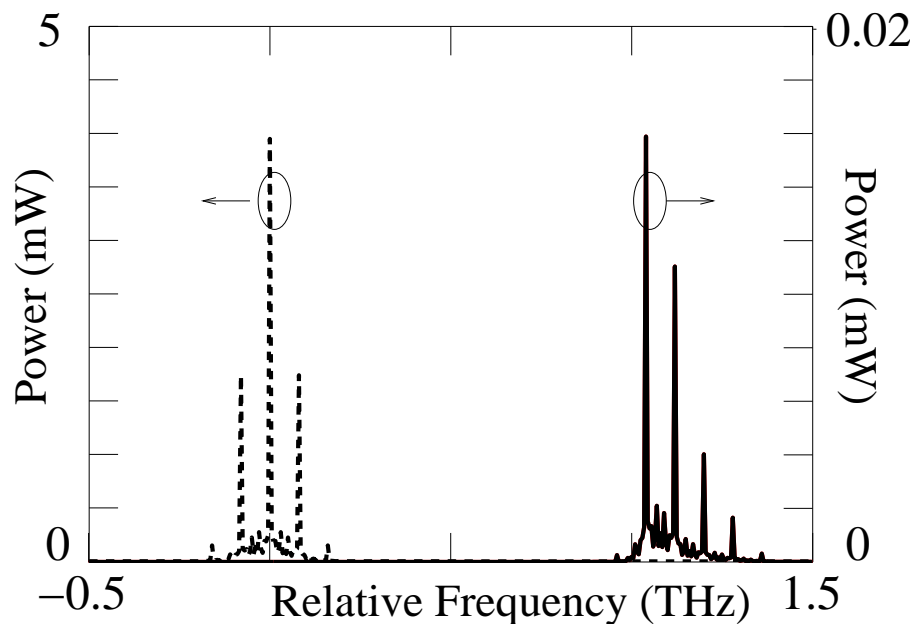


Fig. 4.5: Frequency spectra before propagation through the transmission system. The spectrum of the original signal is shown with a dashed line and that of the wavelength-converted signal is shown with a solid line.

with a dashed line and that of the wavelength-converted signal before the pre-amplifier with a solid line. The power scale for the standard signal is given on the left side of the plot, while that of the frequency-converted signal is shown on the right side. In particular, the power of the wavelength-converted signal is about two orders of magnitude smaller than that of the original signal. We observe that the original CW signal together with the low-frequency half of the wavelength-converted signal has been filtered out by the band-pass filter. The side tones generated due to XPM can be clearly seen.

In Fig. 4.6, the dashed curve shows a portion of the time sequence of the wavelength-converted signal and the solid curve shows the standard signal,

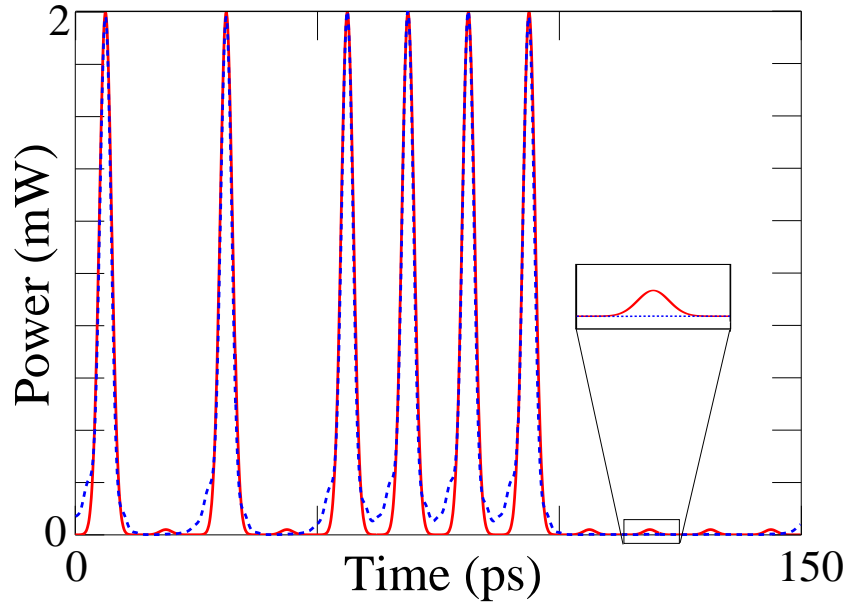


Fig. 4.6: The time sequence after wavelength conversion. The solid red curve is from the standard transmitter and the dashed blue curve is that of the wavelength-converted signal. The inset shows an isolated space.

both after the pre-amplifier. The inset in Fig. 4.6 shows an expansion of a zero bit before and after wavelength conversion. Figure 4.6 shows that the full-width half maximum (FWHM) pulsewidth of the wavelength-converted signal is maintained at 3 ps. It is important for the wavelength converter to maintain the pulsewidth in order to reduce any possible intersymbol interference (ISI) that may accumulate over the propagation spans. Wavelength conversion also improves the extinction ratio, in agreement with what was seen in the experiments [24].

The two signals are then propagated through the transmission system. The signal is received using the same pre-amplified receiver described ear-

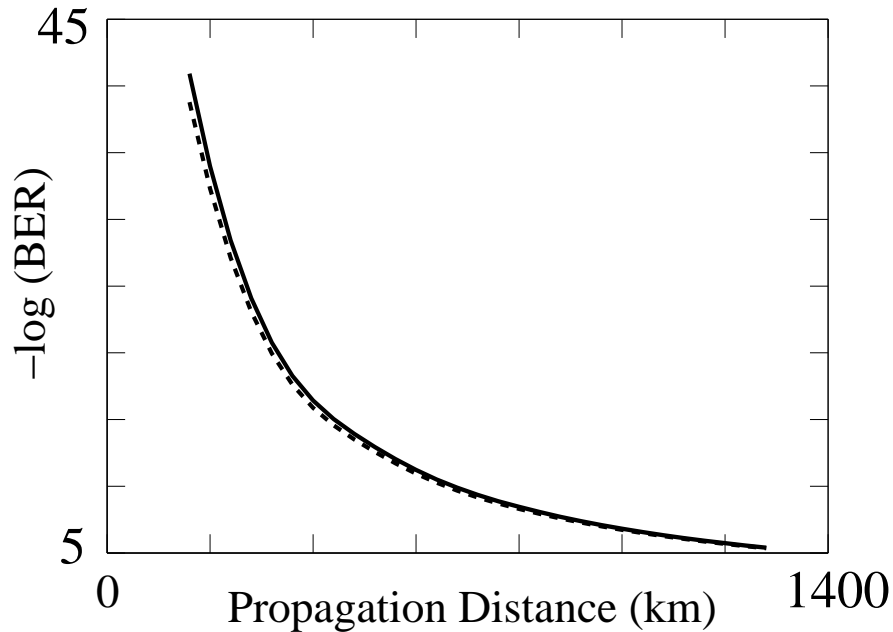


Fig. 4.7: The BER as a function of propagation distance. The solid line shows the BER for the wavelength-converted signal and the dashed line shows the BER for the standard 80-Gb/s signal.

lier, consisting of a supergaussian optical filter, a square-law photodetector, and an electrical filter with fifth-order Bessel transfer function. The BER is computed from the average probability density functions (pdfs) of marks and spaces which are obtained by averaging the Gaussian approximations to the pdfs in each of the marks and spaces [28, 29]. The BER of the wavelength-converted signal is then compared to that of the standard signal. The BER as a function of propagation distance is shown in Fig. 4.7. The BER of the wavelength-converted signal is shown with a solid line, and that of the standard signal with a dashed line.

The BER of the wavelength-converted signal is slightly less than that of the standard signal. The reason is that the optical extinction ratio in

the spaces of the standard signal is 20 dB, whereas that of the wavelength-converted signal is about 30 dB, which can be seen in the inset in Fig. 4.6. As a result, the variance due to signal-noise beating in the spaces is somewhat smaller for the wavelength-converted signal than for the standard signal. This improvement in the extinction ratio is consistent with the observations in [24], and it more than compensates for a slight degradation in the shape of the pulse in the marks that occurs during wavelength conversion. After 1000 km propagation through the system both signals have a BER of about 10^{-7} . These results clearly indicate that wavelength conversion by XPM leads to no appreciable degradation in a noise-limited system.

5. CONCLUSIONS

Wavelength conversion is an important signal processing application, which has numerous uses in long-haul optical networks. Numerous all-optical wavelength conversion techniques have been proposed and experimental demonstrated. The techniques demonstrated to date include cross-gain modulation in a semiconductor optical amplifier (SOA) [22], cross-phase modulation (XPM) in a non-linear optical loop mirror [20], and regenerative techniques [15]. I described these techniques, and I discussed their advantages and disadvantages.

For best performance in a high speed optical communication system, phase coherence is important. All-optical wavelength conversion utilizing XPM in fibers can help improve the phase correlation, as well as improve the extinction ratio [24]. Hence, this method is a strong candidate for wavelength conversion in long-haul, network systems. However, previous studies do not account for the tolerance of the signal to long-haul propagation. I modeled the wavelength conversion process, as well as the transmission system, in order to study the effects of propagation.

The BER after 1280 km of propagation of the wavelength converted signal at 80-Gb/s were calculated. We found a slight improvement from the result when an unconverted signal is propagated. The slight improvement in BER

in the case of the wavelength converted signal is due to an improvement in the extinction ratio, causing a decrease in the standard deviation in the spaces, and leading to improved BERs. Hence, wavelength conversion leads to no significant deterioration in a noise-limited propagation system. In future work, we will investigate the performance when several wavelength converters are concatenated in a network.

Appendix A: LIST OF ACRONYMS

ASE	Amplifier spontaneous emission
BER	Bit-error ratio
BPF	Band-pass filter
CW	Continuous wave
DCF	Dispersion compensating fiber
DSF	Dispersion shifted fiber
EDFA	Erbium-doped fiber amplifier
FFT	Fast-Fourier transform
FWHM	Full width at half maximum
FWM	Four wave mixing
GVD	Group velocity dispersion
HNL-DSF	High-nonlinearity dispersion shifted fiber
ISI	Intersymbol interference
MZI	Mach Zehnder interferometer
NLSE	Nonlinear Schrödinger equation
NOLM	Nonlinear optical loop mirror
OPA	Optical parametric amplifier
OTDM	Optical time division multiplexing

RZ	Return-to-zero
SBS	Stimulated Brillouin scattering
SMF	Single mode fiber
SNR	Signal-to-noise ratio
SOA	Semiconductor optical amplifier
SPM	Self-phase modulation
SRS	Stimulated Raman scattering
WDM	Wavelength-division multiplexing
XGM	Cross-gain modulation
XPM	Cross-phase modulation

BIBLIOGRAPHY

- [1] G. P. Agrawal, *Fiber-optic Communication Systems* (John Wiley & Sons, 2002).
- [2] R. Ramaswami, and K. N. Sivarajan, *Optical Networks* (Morgan Kaufmann, 2002).
- [3] L. Kazovsky, S. Benedetto, and A. Willner, *Optical Fiber Communication Systems* (Artech House).
- [4] G. P. Agrawal, *Nonlinear Fiber Optics* (Academic, 1995).
- [5] K. -P. Ho, *Phase-modulated Optical Communication Systems* (Springer).
- [6] Y. R. Shen, *The Principles of Nonlinear Optics* (John Wiley & Sons, 1984).
- [7] R. Holzlohner, “A covariance matrix method for the computation of bit errors in optical transmission systems,” Ph.D. Dissertation, Univ. Maryland Baltimore County (2003).
- [8] C. R. Menyuk, “Application of multiple-length-scale methods to the study of optical fiber fiber transmission,” *J. Eng. Math.* **36**, 113–136 (1999).

- [9] O. V. Sinkin, R. Holzlöhner, J. Zweck, and C. R. Menyuk, “Optimization of the split-step Fourier method in modeling optical-fiber communication systems,” *J. Lightwave Technol.* **21**, 61–68 (2003).
- [10] J. M. H. Elmirghani, and H. T. Mouftah, “All-optical wavelength conversion: Technologies and applications in DWDM networks,” *IEEE Commun. Mag.* 86–92 (2000).
- [11] M. J. Offside, J. E. Carroll, M. E. Bray, and A. Hadjifotiou, “Optical wavelength converters,” *IEE Opt. Commun.* 59–71 (1995).
- [12] P. Öhlén, and E. Berglind, “BER caused by jitter and amplitude noise in limiting optoelectronic repeaters with excess bandwidth,” *IEE Proc. Optoelectron.* **145**, 147–150 (1998).
- [13] D. Wolfson, A. Kloch, T. Fjelde, C. Janz, B. Dagens, and M. Renaud, “40-Gb/s all-optical wavelength conversion, regeneration, and demultiplexing in an SOA-based all-active Mach–Zehnder interferometer,” *Photon. Technol. Lett.* **12**, 332–334 (2000).
- [14] O. Brox, A. Kilk, C. Caspar, D. Hoffmann, M. Mohrle, G. Sahin, and B. Sartorius, “Q-Switched laser module for regenerative wavelength conversion,” *Proc. Eur. Conf. Optical Commun.* **2**, 57–58 (2000).
- [15] F. Devaux, “All-optical 3R regenerators : status and challenges,” *International Semiconductor Laser Conference*, 5–6 (2000).
- [16] S. Fischer, M. Dulk, E. Gamper, W. Vogt, E. Gini, H. Melchior, W.

- Hunziker, D. Nasset, and A. D. Ellis, “Optical 3R regenerator for 40 Gb/s networks,” *Electron. Lett.* **35**, 2047–2049 (1999).
- [17] T. Durhuus, B. Mikkelsen, C. Joergensen, S. L. Danielsen, and K. E. Stubkjaer, “All-optical wavelength conversion by semiconductor optical amplifiers,” *J. Lightwave Tech.* **14**, 942–954 (1996).
- [18] J. Leuthold, L. Moller, J. Jaques, S. Cabot, L. Zhang, P. Bernasconi, M. Cappuzzo, L. Gomez, E. Laskowski, E. Chen, A. Wong-Foy and A. Griffin, “160 Gbit/s SOA all-optical wavelength converter and assessment of its regenerative properties,” *Electron. Lett.* **40**, 554–555 (2004).
- [19] R. Sabells, E. Iannone, and E. Pagano, “Optical transport networks employing all-optical wavelength conversion: Limits and features,” *J. Selected Commun.* **14**, 968–978 (1996).
- [20] D. M. Patrick, A. D. Ellis, and D. M. Spirit, “Bit-rate flexible all-optical demultiplexing using a nonlinear optical loop mirror,” *Electron. Lett.* **29**, 702–703 (1993).
- [21] C. Langrock, S. Kumar, J. E. McGeehan, A. E. Willner, and M. M. Fejer, “All-optical signal processing using $\chi^{(2)}$ nonlinearities in guided-wave devices,” *J. Lightwave Tech.* **24**, 2579–2592 (2006).
- [22] A. Mecozzi, “Small-signal theory of wavelength converters based on cross-gain modulation in semiconductor optical amplifiers,” *IEEE Photon. Technol. Lett.* **8**, 1471–1473 (1996).
- [23] B.-E. Olsson, P. Öhlén, L. Rau, and D.J. Blumenthal, “A simple and

- robust 40-Gb/s wavelength converter using cross-phase modulation and optical filtering,” *IEEE Photon. Technol. Lett.* **12**, 846–848 (2000).
- [24] L. Rau, W. Wang, S. Camatel, H. Poulsen, and D.J. Blumenthal, “All-optical 160-Gb/s phase reconstructing wavelength conversion using cross-phase modulation (XPM) in dispersion-shifted fiber,” *IEEE Photon. Technol. Lett.* **16**, 2520–2522 (2004).
- [25] J. H. Lee, Z. Yusoff, W. Belardi, M. Ibsen, T. M. Monro, and D. J. Richardson, “A tunable WDM wavelength converter based on cross-phase modulation effects in normal dispersion holey fiber,” *IEEE Photon. Technol. Lett.* **15**, 437–439 (2003).
- [26] J. Herrera, F. Ramos, and J. Marti, “Small-signal analysis of wavelength converters based on cross-phase modulation in dispersion-shifted fibers,” *IEEE Photon. Technol. Lett.* **17**, 2370–2372 (2005).
- [27] D. Marcuse, “Derivation of analytical expressions for the bit-error probability in lightwave systems with optical amplifiers,” *J. Lightwave Technol.* **8**, 1816–1823 (1990).
- [28] I.T. Lima, Jr., A.O. Lima, Y. Sun, H. Jiao, J. Zweck, C.R. Menyuk, and G.M. Carter, “A receiver model for optical fiber communication systems with arbitrarily polarized noise,” *J. Lightwave Technol.* **23**, 1478–1490 (2005).
- [29] P. Griggio, J. Hu, J. Wen, G. E. Tudury, J. Zweck, B. S. Marks, L. Yan, G. M. Carter, and C. R. Menyuk, “Characterizing pattern dependence in

transmitters and receivers for modeling optical communication systems,”
Opt. Commun. **272**, 107–110 (2007).

